Study of rail-wheel contact problem by analytical and numerical approaches

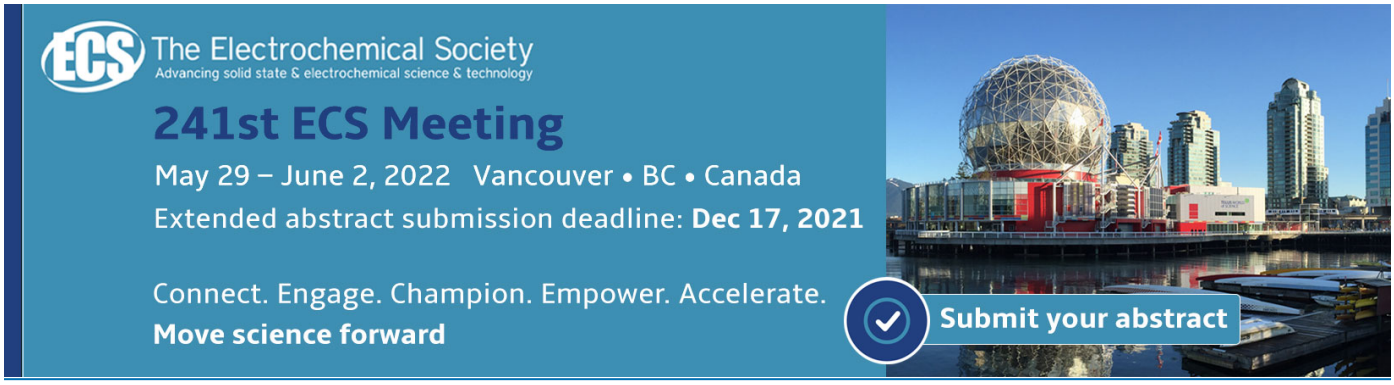

Study of rail-wheel contact problem by analytical and numerical approaches

G G Sirata [1,3,*], H G Lemu[2] K Wacławiak[3] and Y D Jelila[1,4]

[1] Faculty of Mechanical Engineering, Jimma University, Ethiopia
[2] Faculty of Science and Technology, University of Stavanger, Norway
[3] Silesian University of Technology, Department of Materials Technologies, Poland
[4] Silesian University of Technology, Department of Transport Systems, Traffic Engineering and Logistics, Poland

[*] Corresponding author e-mail: goftilagudeta@gmail.com

Abstract. This study presents the rail wheel contact problems under normal and tangential categories. Both analytical and numerical approaches were used for modelling, where the analytical approach assumed elliptical contact patches based on the Hertz theory. In the numerical approach, 3D finite element models were used to investigate non-elliptical contact patches. The only elastic material model was considered in the case of Hertz theory. However, in the case of finite element analysis, both elastic and elastoplastic material models were used to simulate the material's behavior under the applied load. The elastoplastic material model was used to determine the amount of stress at which the plastic deformation starts, which enables determining the rail wheel's critical load. The commercial software ABAQUS was employed for 3D modeling and contact stress analysis. The study shows maximum stress at 3 mm from the rail wheel contact surface when the maximum load of 85 kN is applied. This initiates the cracks in the subsurface and causes the portion of the rail wheel to break off in the form of spalling after a certain time.

1. Introduction

In comparison to other modes of transportation, railway transport is now well recognized for its low cost, efficiency, environmental friendliness, and high speed [1]. As a result, it has played a vital role in solving transport problems and integrating cities and countries for decades. However, despite its decades-long history and advancements in rail and train safety, catastrophic disasters still occur frequently due to rail wheel failures. Failure mechanisms such as wear, plastic deformation, and rolling contact fatigue significantly reduce the life of the rail wheel. Among these failure mechanisms, rolling contact fatigue plays a predominant role. This is the result of repeated contact stresses and creep forces acting on the contact area of the rail wheel. When the contact stress exceeds a threshold value, rolling contact fatigue crack forms at the surface or subsurface level. For example, creep forces cause the accumulation of the plastic strain on the surface of the rail wheel and subsequently form surface cracks. However, the growth of the surface crack depends on the existing wear rate. Thus, the surface crack can extend below the surface and cause failure if low wear rate. Conversely, if the wear rate is excessive, the surface crack may not grow beneath the surface of the rail wheel because the wear dominates the crack.

In the same way, high wheel loads cause high compressive stress at a certain depth below the surface of the rail wheel. Due to this high compressive stress, the plastic strain may accumulate at the subsurface level and initiate the subsurface crack over time. Subsurface crack is very dangerous since it detaches the portion of the rail wheel in the form of spalling and causes catastrophic failure of the rail wheel without showing any warning. Therefore, analyzing the stress distribution and determining where a subsurface crack can initiate due to cyclic rolling contact is crucial in establishing the structural integrity of the rail wheel. This analysis depends on the applied forces, contact geometry, and material behavior that significantly affect the rolling contact interaction [2,3].

Rail-wheel contact is commonly considered as a contact between two quasi-identical bodies and can be divided into normal and tangential contact [4–6]. In the normal contact problem, the contact patch's size, shape, and position and the normal pressure distribution within the contact patch are determined from the rail-wheel geometry and normal force [7]. The normal contact problem is mainly investigated based on Heinrich Hertz's elastic theory [8]. Many researchers in most rail wheel contact modelling have frequently used Hertz's theory, which depends on elastic mechanical properties and can be applied to spherical, cylindrical, and elliptical contacts [9–12]. Yan and Fischer [13] used Hertz's theory to analyze the rail-wheel contact problem. In the tangential contact problem, the relationship between tangential forces and creepages is analyzed. Besides the normal stresses, the shear stresses between contacting surfaces are also determined under the tangential contact problem. Various researchers also studied tangential contact problems since the normal contact phenomena alone cannot fully describe the rail-wheel contact problem. Kalker [14] proposed a hypothesis that considers linearity for determining the rail wheel's tangential forces and spin moment. This model is valid for small lateral, longitudinal, and spin creepages and serves as a foundation for tangential rolling contact analysis. Polach [15] also presents the relationship between the tangential traction force, creepage, and friction force. However, these contact theories do not consider the elastoplasticity deformation of the material.

In order to consider the elastoplastic deformation of the material, a few studies used numerical methods. Arslan and Kayabaş [16] investigated the wheel-rail contact problem using finite element analysis methods and compared the results with real-life problems experienced in wheel contact. Tao et al. [17] proposed a 3D model to study the normal and tangential stress distribution in the contact surface of rail wheels. Khoa [7] employed a 3D finite element model of elastoplastic material to investigate stress distribution and material response under various adhesion circumstances. Wiest et al. [18] used a FE analysis to determine the wheel-rail contact problem's contact pressure, surface area, and penetration depth. Ma et al. [19] employed an explicit finite element method to analyze contact instabilities between rail and wheel and provided contact solutions based on the area of the contact patches and the normal pressure distribution.

This study focuses on the rail wheel rolling contact problems under normal and tangential categories. Numerical approach is employed to simulate the material behaviour under both categories. The aim is to use position of the maximum effective stress to identify where the rolling contact fatigue crack can be initiated. Furthermore, the study intends to determine the magnitude of the stresses and deformations and the contact area's size and shape in both approaches. While the Hertzian contact theory was used to compare the results of the normal direction analytical solutions with numerical results, Kalkers theory [14] and Polach theory [15] were used for the analytical study of the tangential contact problem. Finally, the analytical results were compared with the numerical results carried out by the commercial tool ABAQUS and the obtained results are discussed.

2. Materials and methods

2.1. Rail-Wheel material

In both the normal and tangential contact analysis, the properties of the linear elastic material of the rail wheel were considered. Steel is the material commonly used to manufacture rails and wheels, whose elastic properties are listed in Table 1. In the case of numerical modelling, both elastic and elastoplastic material properties were considered.

Table 1. Rail wheel elastic material properties [10]

Mechanical properties	Wheel	Rail
Poisson ratio,-	0.3	0.3
Young's modulus, GPa	206	200
Density, kg/m^3	7,850	7,850

2.2. Model of rail-wheel surface geometry

To determine the rail wheel contact parameters under normal contact problem, the four main curvature of half-spaces $R_x^{(w)}$, $R_y^{(w)}$, $R_x^{(r)}$ and, $R_y^{(r)}$, are illustrated in Figure 1, where $R_x^{(w)}$ and $R_y^{(w)}$ are the radii of curvature of the wheel along the x and y-axis, and $R_x^{(r)}$ and, $R_y^{(r)}$ are the radii of curvature of the rail along the x and y-axis, respectively. $\frac{1}{R_x}$, and $\frac{1}{R_y}$ represent composite radii, which can be defined by equation (1). In this study, the effect of conicity is ignored since its influence is minimal. Therefore, $R_x^{(w)}$ and $R_y^{(r)}$ are assumed to be the wheel's rolling and the railhead's radius, respectively.

$$\frac{1}{R_x}=\frac{1}{R_x^{(w)}}=2A; \qquad \frac{1}{R_y}=\frac{1}{R_y^{(w)}}+\frac{1}{R_y^{(r)}}=2B \tag{1}$$

Where A and B describe the radius of the rail-wheel and radius of curvature respectively.

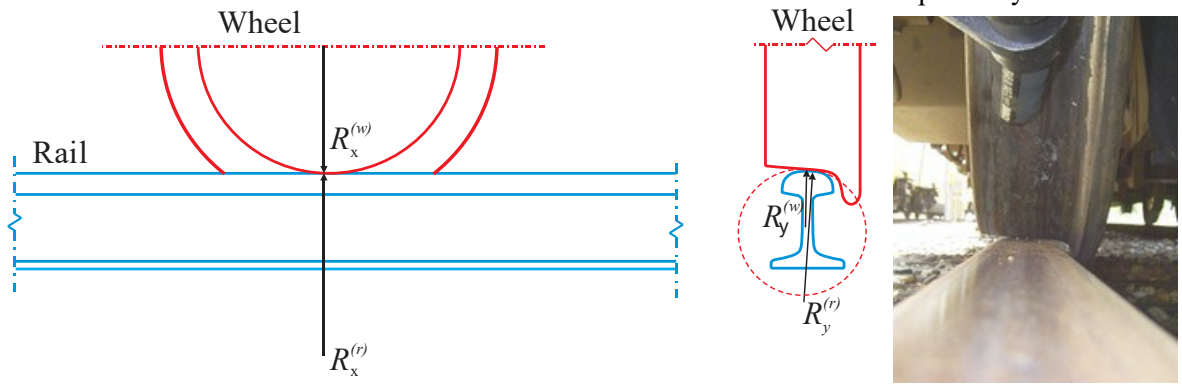

Figure 1. Wheel–rail configuration showing different principal relative radii of curvature

3. Analytical analysis

3.1. Normal contact modelling

The most commonly used analytical method for solving normal contact problems is the Hertzian contact theory. In Hertzian contact theory, the contact patch of the rail-wheel is assumed to be elliptical in shape. The contact patch and pressure distribution can be determined based on Hertz's assumption.

3.1.1. Elliptical contact patch. The semi-axis 'a' and 'b' of the contact ellipse are dependent on material properties, the rail-wheel geometry, and the prescribed force and also given by equations (2) and (3). Figure 2 shows the elliptical contact patch of the rail wheel.

$$a=m\left(\frac{3}{4}\frac{F_n}{E^*}\frac{1}{A+B}\right)^{\frac{1}{3}}$$
$$b=n\left(\frac{3}{4}\frac{F_n}{E^*}\frac{1}{A+B}\right)^{\frac{1}{3}} \tag{2}$$

$$\frac{1}{E^*} = \frac{1-\nu_w^{\,2}}{E_w} + \frac{1-\nu_r^{\,2}}{E_r} \tag{3}$$

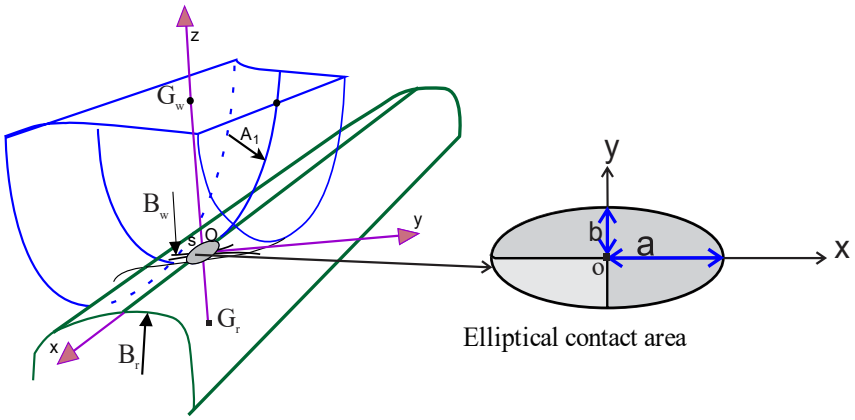

Figure 2. Elliptical contact patch in the rail-wheel interaction

Hence, with E_w, E_r and ν_w, ν_r, being the modulus of elasticity and Poisson's ratios of the wheel and rail, respectively; m and n are coefficients for semi-axis lengths of the ellipse, which was tabulated by Hertz as a function of the ratio $g = n/m$. The geometrical dependency is defined by using an intermediate parameter, angle 'θ' and determined by equation (4):

$$\cos\theta = \frac{|B-A|}{A+B} \tag{4}$$

Knowing an intermediate parameter θ, the Hertzian non-dimensional coefficients, m, n, and r can be found by using a pre-calculated table as shown in Table 2.

Table 2. Hertz coefficients for $A/B < 1$

$\theta°$	90	80	70	60	50	40	30	20	10	0
g	1	0.7916	0.6225	0.4828	0.3652	0.2656	0.1806	0.1080	0.047	0
m	1	1.128	1.285	1.486	1.754	2.136	2.731	3.816	6.612	∞
n	1	0.8927	0.8000	0.7171	0.6407	0.5673	0.4931	0.4122	0.311	0
r	1	0.9932	0.9726	0.9376	0.8867	0.8177	0.7263	0.6038	0.428	0

Considering the wheel with the rolling radius $R_x^{(r)} = 430$ mm and the rail with the radius of the head $R_y^{(r)} = 300$ mm, $R_y^{(w)} = 510$ mm, then $R_x^{(w)}$ becomes infinity (i.e., $1/R_x^{(r)} = 0$) since the rail is assumed to be straight. $A + B$ and $B - A$ can be calculated from the above equations and becomes 0.00283 and 0.0005 respectively (i.e. A = 0.0038 and B = 0.00168). An intermediate parameter, the angle, θ can be found by substituting A+B and B-A values into equation (4), whose value becomes 63.76°. The values of m and n are 1.38 and 0.76, respectively. These values could be obtained from Table 2 at $\theta = 63.76°$. Assuming the maximum load on a single wheel is approximately equal to F_n = 85 kN, the values of the contact patch 'a' and 'b' was found to be 7.11 mm and 4.12 mm, respectively.

3.1.2. Pressure distribution in the contact patch. The contact pressure distribution, P(x,y), is applied over the contact area, defined by equation (5). It highly depends on the normal load, F_n.

$$P(x,y) = \frac{3}{2\pi ab} F_n \sqrt{1 - \left(\frac{x}{a}\right)^2 - \left(\frac{y}{b}\right)^2} \tag{5}$$

Substituting the values of F_n = 85 kN, a = 7.11 mm, and b = 4.12 mm into equation (5), the maximum normal contact pressure at the center of the contact patch is 1386 MPa. The semi ellipsoidal normal contact pressure distribution is plotted along the major and minor diameter of the contact ellipse and illustrated in Figure 3.

3.2. Tangential contact modelling

The tangential contact problem comprises the creep forces and the relative motion between the rail and the wheel. Kalker's linear theory [14] and Polach's tangential theory [15] are used to analyze the tangential contact problem of the rail wheel. In this study, the rail is assumed to be straight and, thus, only pure longitudinal creepage (ξ), which is defined by equation (6), is considered. Therefore, lateral creepage, η, and spin creepage Ω are ignored.

$$Longitudinal\ creepage, \xi = \frac{v_{long}}{v_{rolling}} = \frac{v_x^{(w)} - v_x}{v_{rolling}} \tag{6}$$

where, v_{log} is the creep velocity in the longitudinal direction, $v_{rolling}$ is the rolling velocity.

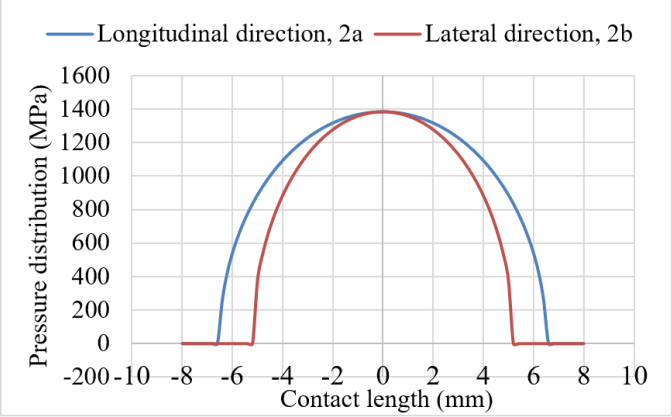

Figure 3. Semi-ellipsoidal contact pressure along the longitudinal and lateral direction

The longitudinal creep force F_x, which develop between the rail and wheel can be determined by equation (7)

$$F_x = -GC_{11}ab\xi \tag{7}$$

where a and b are the contact patch's elliptical semi-axes, G is the combined shear modulus of rigidity of the rail and wheel materials, C_{11} is called Kalker's creep coefficient obtained by equation (8).

$$C_{11} = 3.2893 + \frac{0.975}{b/a} - \frac{0.012}{\left(b/a\right)^2} \tag{8}$$

Then the combined modulus of rigidity for the rail and wheel can be obtained using equation (9)

$$\frac{1}{G} = \left(\frac{1-v_w^2}{G_w} + \frac{1-v_r^2}{G_r}\right) \tag{9}$$

where, G_r and G_w are the shear modulus; v_r and v_w are the Poisson's ratios of the rail and the wheel, respectively.

Polach's theory [15] also describes the tangential traction force (Q) by considering the relationship between creepage and friction coefficients. In this theory, the elliptical contact is assumed to be divided to stick and slip regions. Thus, the tangential traction force is defined as

$$Q = \frac{2\mu F_n}{\pi}\left(\frac{\varepsilon}{1+\varepsilon^2} + \arctan\varepsilon\right) \tag{10}$$

where, F_n is wheel load, μ is coefficient of friction, ε is a gradient of the tangential and is obtained by equation (11).

$$\varepsilon = \frac{2}{3}\left(\frac{G\pi abc_{ij}}{F_n\mu}\right) \tag{11}$$

where c_{ij} is the longitudinal creepage coefficient given by equation (12).

$$c_{ij} = c_{11} \times \xi \tag{12}$$

Inserting the value of the longitudinal creepage ξ, which is calculated as 0.001 and the value of C_{11} found from equation (8), equation (12) gives $C_{ij} = 4.22$.

Based on the Khoa assumptions, this study considered three cases to describe the relationship between the traction force and the longitudinal creepage [7]. (1) Case 1: Grease lubricated condition $\mu = 0.05$, (2) Case 2: Water lubricated condition$\mu = 0.2$, and (3) Case 3: Dry wheel-rail contact condition$\mu = 0.45$.

The traction force vs. the longitudinal creepage is plotted in Figure 4 for the three above cases of rail-wheel contact conditions. The result shows that the traction force increases with the longitudinal creepage up to a specific value and then becomes almost constant. It can also be observed that the traction force increases as the friction coefficient increases.

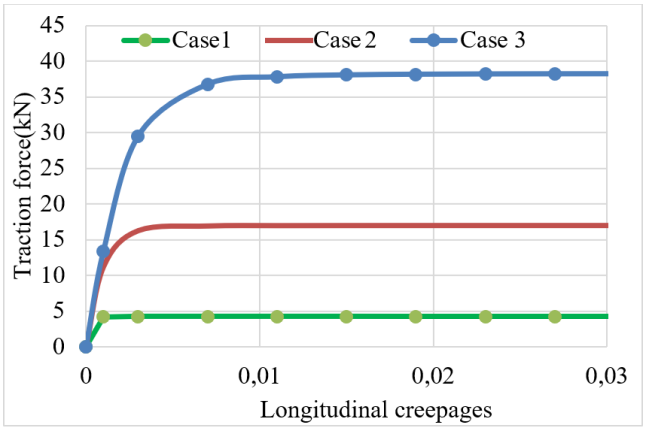

Figure 4. Traction vs longitudinal creepages for different contact conditions

4. Finite element analysis

4.1. Normal contact conditions

The sub-modeling technique was used for its efficiency at fine meshes. Figures 5 and 6 show the normal contact pressure distribution of the FE sub-model for the wheel tread and railhead, respectively. The maximum normal contact pressures are 1427 MPa and 1454 MPa for the rail and wheel, respectively.

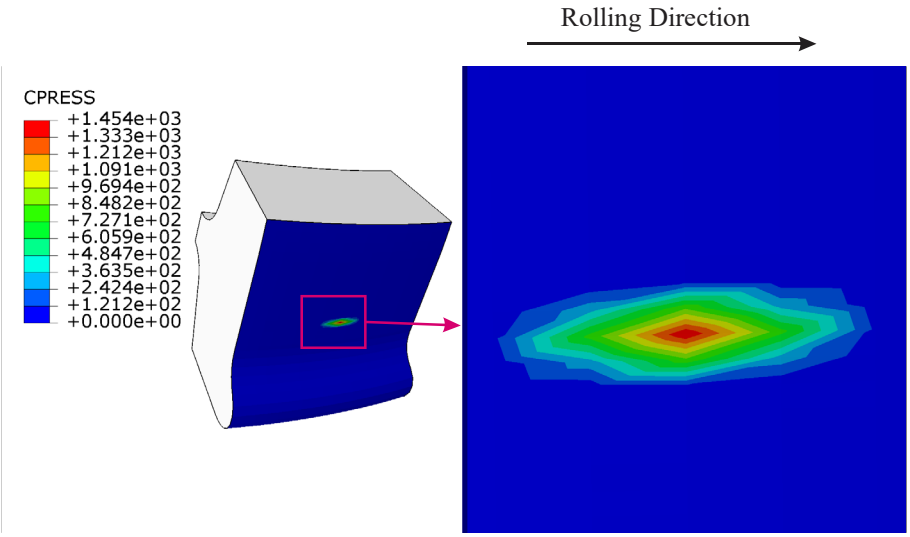

Figure 5. Contour plot of contact pressure distribution on the wheel

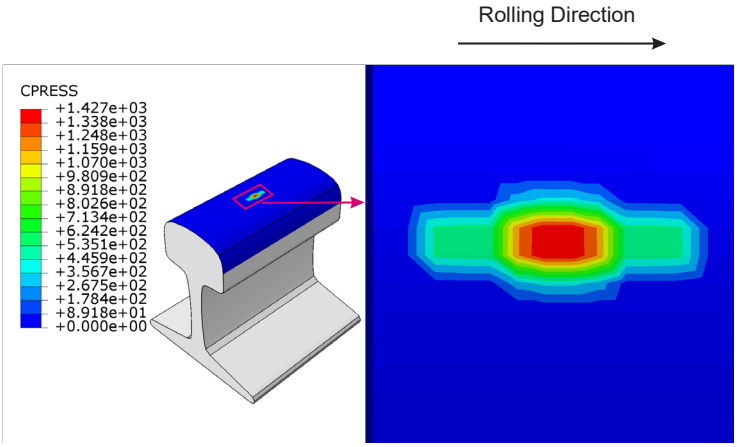

Figure 6. Contour plot of contact pressure distribution on the rail.

Figure 7 shows the normal contact pressure distributions on the wheel tread along with longitudinal and lateral directions in the FE sub-model.

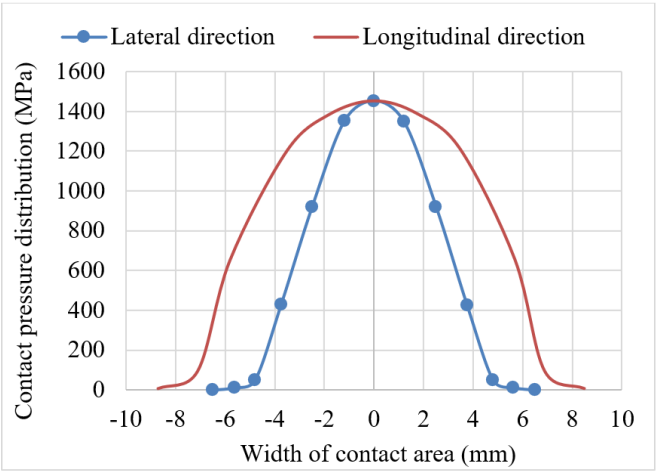

Figure 7. Pressure distribution along with longitudinal and lateral distribution from FE result

4.1.1. Von-Mises stress distribution. The von Mises stress distribution is illustrated in Figure 8. The maximum von Mises stress value obtained is 8371 MPa, which is extremely high likely due to localized stress concentration at sharp edge. Figure 9 shows the von Mises stress distribution along the z-direction from the center of the contact surface. This curve clearly shows that the maximum von-Mises stress occurs at the depth between 2 and 4 mm from the contact surface. This is the main cause for the sub-surface fatigue crack initiation, which later propagate to the surface and cause wheel failure.

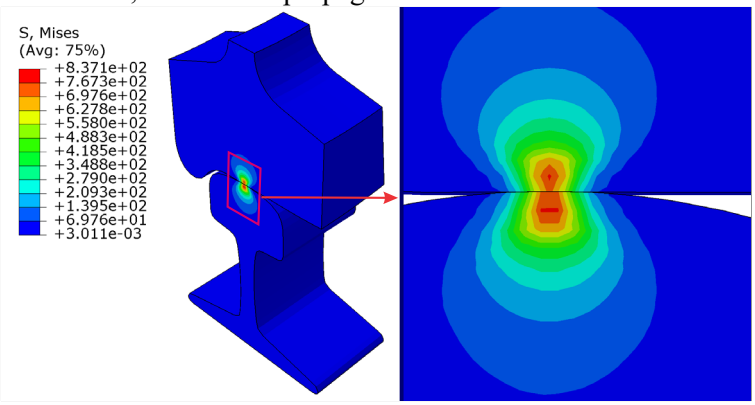

Figure 8. von-Mises stress distribution in the cross-section view rail and wheel

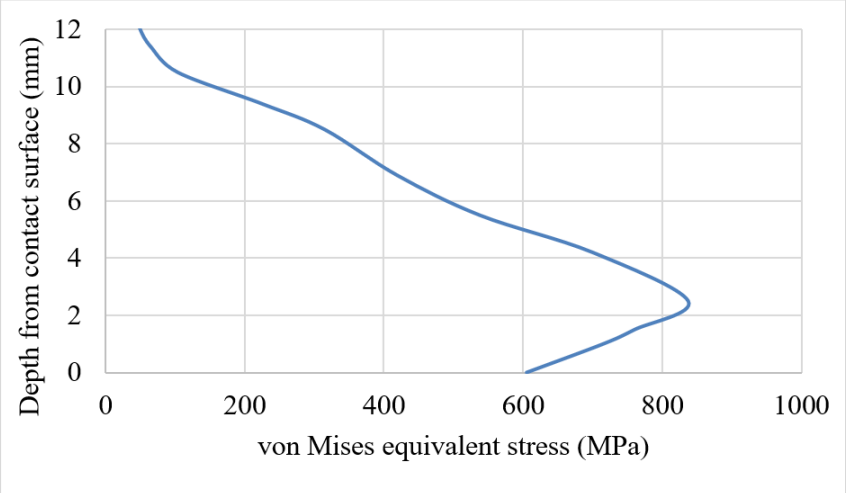

Figure 9. von-Mises stress distribution in the wheel along the vertical direction

4.2. Tangential contact condition

FE model was used to analyze two conditions of the tangential contact problem: 1) Partial slip condition and 2) Full slip conditions. In tangential contact conditions, both the normal pressure distribution and tangential traction distribution have to be applied. Since the track is assumed to be straight, the lateral η and spin creepages φ are ignored, and thus only longitudinal creepage ξ is considered in this study. Two values of longitudinal creepage ξ are taken from [7]: 0.47% for partial slip and 1.2% for a full slip to investigate the creepages' effect on the contact stresses. Additionally, $\mu = 0.2$ frictional coefficient was applied between the rail and wheel.

The FE analysis of the pressure and the shear stress distribution along the moving direction in the case of the partial slip is illustrated in Figure 10. In this figure, it is clearly shown that the shear stress reaches the traction bound in the slip region only.

In the full slip condition, shear stress distribution reaches the traction bound over the contact area. Furthermore, the maximum shear stress that occurred in the full slip condition was higher than in the partial slip condition. The partial sliding and full sliding condition results are summarized in Table 3.

Table 3. FE results of tangential contact conditions

	Partial sliding	Full sliding
Maximum shear stress, MPa	480	530
Maximum Pressure, MPa	1454	1454
Traction force, kN	34.2	38.2

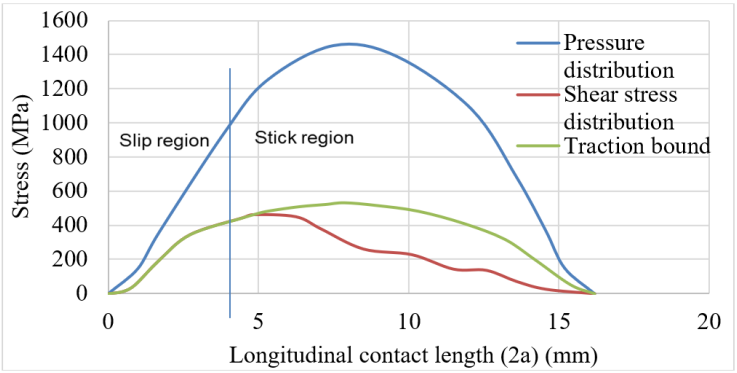

Figure 10. Pressure and shear stress distribution along moving direction for the partial slip

5. Discussion

In this section, analytical computation results are compared with finite element results. The values of half-length 'a' and half-width 'b' of the contact area, as well as the maximum contact pressure, are summarized in Table 4. These comparisons show that the results obtained from finite element analysis almost approach to analytical (Hertz's approaches) results.

Table 4. Analytical and FEM results

Descriptions	Hertz analytical	FEM	Deviation in percent
Major contact width (a), mm	7.0	8.1	13.5 %
Minor contact (b), mm	4.1	4.4	6.8 %
Maximum pressure, MPa	1386	1454	4.6 %

Figure 11 shows the numerical results of maximum normal contact pressure distribution on the wheel versus wheel load for both elastic and elastoplastic material models and also for Hertzian theory. The results show that the maximum normal contact pressure (P_0) increases with the increasing wheel load, L in the case of both elastic and elastoplastic FE model and Hertzian theory. From the results, 85 kN can be considered the wheel load's critical values to deform plastically according to the elastoplastic material model. When the wheel load is below the critical values (85 kN), the effect of the plastic deformation is not more visible from the numerical results.

The results from FE model analysis and analytical computation are given in Table 5. The analyses are based on a wheel load of 85 kN. The results show that the traction force obtained from both FE model and analytical calculations almost approach each other. As the levels of creepage increase, the traction force also increases. The maximum pressure obtained is 1232 MPa and 1229 MPa for the low and high adhesion, respectively.

Table 5. Tangential contact force between rail and wheel.

Approaches	Traction force (kN)	
	Partial slips	Full slips
Polach	38.2	37.8
FEM	34.2	38.2
Deviation	10.7 %	1.2 %

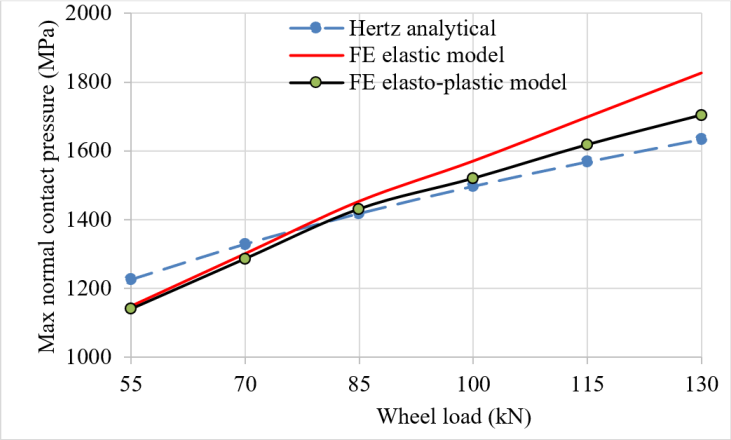

Figure 11 Maximum normal contact pressure (Po) levels versus the wheel loads levels

Polach's approach and FE approach were used to study the influence of creepage on traction forces. For the wheel load of 85 kN and a rolling speed of 80 km/h, the relationship between traction force (or creep force) and creepage under dry contact ($\mu = 0.45$) is illustrated in Figure 12. It was also noticed that the FEM result was slightly lower than Polach's result before the creepage reached the critical value.

When creepage was small, the traction force increased linearly with the creepage. For example, under dry rail-wheel contact conditions, the critical traction force was 37.67 kN for a creepage of 1%.

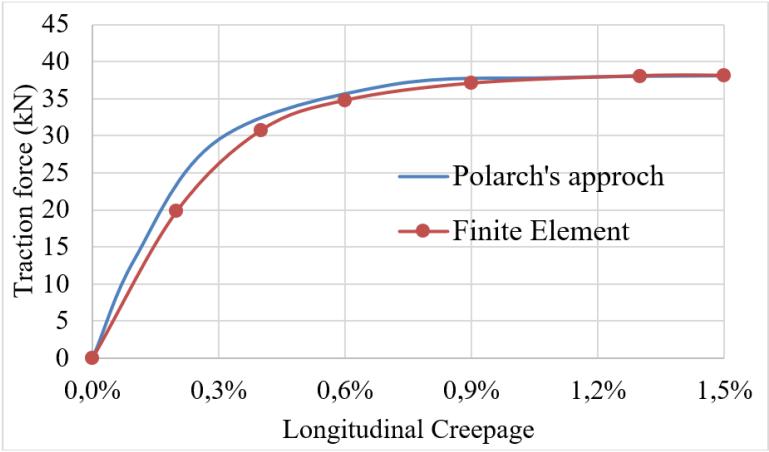

Figure 12 Traction curve for dry contact condition, (friction coefficient = 0.45, F_z = 85 kN)

6. Conclusion

The rail wheel contact problem has been investigated under two categories: 1) normal and 2) tangential contact problems. Normal pressure distribution, contact stresses, contact shape, and size are determined in a normal contact problem. In tangential contact problems, the relationship between creepages and creep forces are investigated. In analytical approaches, Hertzian theory was used to determine these normal contact parameters, and Kalker's and Polarch's models were used to analyze tangential contact problems. In numerical approaches, ABAQUS has been used to analyze both normal and tangential contact problems. In order to reduce computation time, the sub-modeling system was used instead of full modeling. Additionally, to get more accurate results and reduce the computation time, the fine mesh was applied to the parts of the rail-wheel near the contact, and the coarse mesh was applied to other regions of the components. The result shows that the normal pressure distribution increases with the wheel load. From the elastoplastic material behavior, the critical load for the normal contact problem is determined and found to be 85 kN. If the loads exceed 85 kN, the rail-wheel deforms plastically under normal conditions. Under tangential contact conditions, the study shows the traction forces increase the

creepage up to a certain value and then remain constant; however, it continuously increases with the coefficient of friction. The FE analysis also identified where the maximum von Mises is developed. In this study, the maximum von Mises obtained from the FE analysis is 837 MPa, found at a depth between 2 and 4 mm. This demonstrates where a subsurface crack initiates and causes the rail wheel portion to break off in the form of spalling after a certain time.

References

[1] Jelila Y D and Lemu H G 2020 Study of Wheel-Rail Contacts at Railway Turnout Using Multibody Dynamics Simulation Approach. *Int. Workshop Adv. Manuf. Autom*., Springer, p. 371–379.
[2] Özdemir Y and Voltr P 2016 Analysis of the wheel and rail frictionless normal contact considering material parameters. *J Appl Math Comput Mech.* **15(2)**, 95-103.
[3] Srivastava J P, Sarkar P K, and Ranjan V 2014 Contact stress analysis in wheel–rail by Hertzian method and finite element method. *J Inst Eng India Ser C* **95**,319–325.
[4] Sun Y and Ling L 2021 An optimal tangential contact model for wheel-rail non-Hertzian contact analysis and its application in railway vehicle dynamics simulation. *Veh Syst Dyn.* 1–29.
[5] Shackleton P A 2009 An Optimised Wheel-Rail Contact Model for Vehicle Dynamics Simulation. *PhD Thesis. Manchester Metropolitan University.*
[6] Meymand S Z, Keylin A, and Ahmadian M 2016 A survey of wheel–rail contact models for rail vehicles. *Veh Syst Dyn.* **54**:386–428.
[7] Khoa Duy V 2015 Damage analysis of wheel/rail contact associated to high adhesion condition. *PhD Thesis. University of Wollongong.*
[8] Hertz H 1881 On the contact of elastic solids. *Z Reine Angew Math*. **92,**156–71
[9] Knothe K 2008 History of wheel/rail contact mechanics: from Redtenbacher to Kalker. *Veh Syst Dyn.* **46**:9–26
[10] Kalker J J.2018 Survey of wheel-rail rolling contact theory. Dyn. Veh. Roads Tracks Proc. Iavsd Symp. 6th Tech. Univ. Berl. Sept 1979 (p.13), Routledge.
[11] Iwnicki S. 2006 Handbook of railway vehicle dynamics. CRC press.
[12] Barber J. 2018 Contact mechanics, solid mechanics and its applications. Springer, New York.
[13] Yan W and Fischer F D 2000 Applicability of the Hertz contact theory to rail-wheel contact problems. *Arch Appl Mech.* **70**(4), 255-68.
[14] Kalker J.J. 1990 The rolling contact problem. In: Three-dimensional elastic bodies in rolling contact. Solid Mechanics and Its Applications, vol. 2. Springer, Dordrecht.
[15] Polach O 1999 A fast wheel-rail forces calculation computer code. *Veh Syst Dyn.* **33**,728–39
[16] Arslan M A and Kayabaşı O 2012 3-D Rail–Wheel contact analysis using FEA. *Adv Eng Softw.* **45**, 325–31
[17] Tao G, Wen Z, Zhao X, and Jin X 2016 Effects of wheel–rail contact modelling on wheel wear simulation. *Wear* **366**,146–56.
[18] Wiest M, Kassa E, Daves W, Nielsen JCO, and Ossberger H 2008 Assessment of methods for calculating contact pressure in wheel-rail/switch contact. *Wear* **265**, 1439–1445.
[19] Ma Y, Markine V L, Mashal A A, and Ren M 2018 Effect of wheel–rail interface parameters on contact stability in explicit finite element analysis. *Proc Inst Mech Eng Part F J Rail Rapid Transit* **232,** 1879–1894.